Measurement of the Proton Spin Structure Function g_1^p with a Pure Hydrogen Target

The HERMES Collaboration

A. Airapetian[33], N. Akopov[33], I. Akushevich[6], M. Amarian[26,28], E.C. Aschenauer[7], H. Avakian[11], R. Avakian[33], A. Avetissian[33], B. Bains[16], C. Baumgarten[24], M. Beckmann[13], St. Belostotski[27], J.E. Belz[29,30], Th. Benisch[9], S. Bernreuther[9], N. Bianchi[11], J. Blouw[26], H. Böttcher[7], A. Borissov[15], J. Brack[5], S. Brauksiepe[13], B. Braun[9], St. Brons[7], W. Brückner[15], A. Brüll[15], H.J. Bulten[19,26,32], G.P. Capitani[11], P. Carter[4], P. Chumney[25], E. Cisbani[28], G.R. Court[18], P. F. Dalpiaz[10], R. De Leo[3], E. De Sanctis[11], D. De Schepper[2,21], E. Devitsin[23], P.K.A. de Witt Huberts[26], P. Di Nezza[11], M. Düren[9], A. Dvoredsky[4], G. Elbakian[33], J. Ely[5], A. Fantoni[11], A. Fechtchenko[8], M. Ferstl[9], D. Fick[20], K. Fiedler[9], B.W. Filippone[4], H. Fischer[13], B. Fox[5], S. Frabetti[10], J. Franz[13], S. Frullani[28], M.-A. Funk[6], N.D. Gagunashvili[8], H. Gao[2,21], Y. Gärber[7], F. Garibaldi[28], G. Gavrilov[27], P. Geiger[15], V. Gharibyan[33], V. Giordjian[11], A. Golendukhin[6,24], G. Graw[24], O. Grebeniouk[27], P.W. Green[1,30], L.G. Greeniaus[1,30], C. Grosshauser[9], M. Guidal[26], A. Gute[9], W. Haeberli[19], J.-O. Hansen[2], D. Hasch[7], F.H. Heinsius[13], M. Henoch[6], R. Hertenberger[24], Y. Holler[6], R.J. Holt[16], W. Hoprich[15], H. Ihssen[26], M. Iodice[28], A. Izotov[27], H.E. Jackson[2], A. Jgoun[27], R. Kaiser[7,29,30], E. Kinney[5], A. Kisselev[27], P. Kitching[1], H. Kobayashi[31], N. Koch[9,20], K. Königsmann[13], M. Kolstein[26], H. Kolster[24], V. Korotkov[7], W. Korsch[17], V. Kozlov[23], L.H. Kramer[12], V.G. Krivokhijine[8], F. Kümmell[13], M. Kurisuno[31], G. Kyle[25], W. Lachnit[9], W. Lorenzon[22], N.C.R. Makins[16], S.I. Manaenkov[27], F.K. Martens[1], J.W. Martin[21], H. Marukyan[33], F. Masoli[10], A. Mateos[21], M. McAndrew[18], K. McIlhany[4,21], R.D. McKeown[4], F. Meissner[7], F. Menden[30], A. Metz[24], N. Meyners[6], O. Mikloukho[27], C.A. Miller[1,30], M.A. Miller[16], R. Milner[21], V. Mitsyn[8], A. Most[22], V. Muccifora[11], A. Nagaitsev[8], E. Nappi[3], Y. Naryshkin[27], A.M. Nathan[16], F. Neunreither[9], W.-D. Nowak[7], T.G. O'Neill[2], B.R. Owen[16], J. Ouyang[30], V. Papavassiliou[25], S.F. Pate[25], S. Potashov[23], D.H. Potterveld[2], G. Rakness[5], A. Reali[10], R. Redwine[21], A.R. Reolon[11], R. Ristinen[5], K. Rith[9], H. Roloff[7], P. Rossi[11], S. Rudnitsky[22], M. Ruh[13], D. Ryckbosch[14], Y. Sakemi[31], I. Savin[8], C. Scarlett[22], F. Schmidt[9], H. Schmitt[13], G. Schnell[25], K.P. Schüler[6], A. Schwind[7], J. Seibert[13], T.-A. Shibata[31], K. Shibatani[31], T. Shin[21], V. Shutov[8], C. Simani[10] A. Simon[13], K. Sinram[6], P. Slavich[10,11], M. Spengos[6], E. Steffens[9], J. Stenger[9], J. Stewart[18], U. Stoesslein[7], M. Sutter[21], H. Tallini[18], S. Taroian[33], A. Terkulov[23], B. Tipton[21], M. Tytgat[14], G.M. Urciuoli[28], R. van de Vyver[14], J.F.J. van den Brand[26,32], G. van der Steenhoven[26], J.J. van Hunen[26], M.C. Vetterli[29,30], M. Vincter[30], J. Visser[26], E. Volk[15], W. Wander[9,21], S.E. Williamson[16], T. Wise[19], K. Woller[6], S. Yoneyama[31], H. Zohrabian[33]

[1] *Department of Physics, University of Alberta, Edmonton, Alberta T6G 2N2, Canada*
[2] *Physics Division, Argonne National Laboratory, Argonne, Illinois 60439, USA*
[3] *Istituto Nazionale di Fisica Nucleare, Sezione di Bari, 70124 Bari, Italy*
[4] *W.K. Kellogg Radiation Lab, California Institute of Technology, Pasadena, California 91125, USA*
[5] *Nuclear Physics Laboratory, University of Colorado, Boulder, Colorado 80309-0446, USA*
[6] *DESY, Deutsches Elektronen Synchrotron, 22603 Hamburg, Germany*
[7] *DESY Zeuthen, 15738 Zeuthen, Germany*
[8] *Joint Institute for Nuclear Research, 141980 Dubna, Russia*
[9] *Physikalisches Institut, Universität Erlangen-Nürnberg, 91058 Erlangen, Germany*
[10] *Dipartimento di Fisica, Università di Ferrara, 44100 Ferrara, Italy*
[11] *Istituto Nazionale di Fisica Nucleare, Laboratori Nazionali di Frascati, 00044 Frascati, Italy*
[12] *Department of Physics, Florida International University, Miami, Florida 33199, USA*
[13] *Fakultät für Physik, Universität Freiburg, 79104 Freiburg, Germany*
[14] *Department of Subatomic and Radiation Physics, University of Gent, 9000 Gent, Belgium*
[15] *Max-Planck-Institut für Kernphysik, 69029 Heidelberg, Germany*
[16] *Department of Physics, University of Illinois, Urbana, Illinois 61801, USA*
[17] *Department of Physics and Astronomy, University of Kentucky, Lexington, Kentucky 40506, USA*
[18] *Physics Department, University of Liverpool, Liverpool L69 7ZE, United Kingdom*
[19] *Department of Physics, University of Wisconsin-Madison, Madison, Wisconsin 53706, USA*
[20] *Physikalisches Institut, Philipps-Universität Marburg, 35037 Marburg, Germany*
[21] *Laboratory for Nuclear Science, Massachusetts Institute of Technology, Cambridge, Massachusetts 02139, USA*
[22] *Randall Laboratory of Physics, University of Michigan, Ann Arbor, Michigan 48109-1120, USA*
[23] *Lebedev Physical Institute, 117924 Moscow, Russia*
[24] *Sektion Physik, Universität München, 85748 Garching, Germany*
[25] *Department of Physics, New Mexico State University, Las Cruces, New Mexico 88003, USA*
[26] *Nationaal Instituut voor Kernfysica en Hoge-Energiefysica (NIKHEF), 1009 DB Amsterdam, The Netherlands*
[27] *Petersburg Nuclear Physics Institute, 188350 St. Petersburg, Russia*
[28] *Istituto Nazionale di Fisica Nucleare, Sezione Sanità, 00161 Roma, Italy*

[29] *Department of Physics, Simon Fraser University, Burnaby, British Columbia V5A 1S6, Canada*
[30] *TRIUMF, Vancouver, British Columbia V6T 2A3, Canada*
[31] *Tokyo Institute of Technology, Tokyo 152, Japan*
[32] *Department of Physics and Astronomy, Vrije Universiteit, 1081 HV Amsterdam, The Netherlands*
[33] *Yerevan Physics Institute, 375036 Yerevan, Armenia*

A measurement of the proton spin structure function $g_1^{\mathrm{p}}(x, Q^2)$ in deep-inelastic scattering is presented. The data were taken with the 27.6 GeV longitudinally polarised positron beam at HERA incident on a longitudinally polarised pure hydrogen gas target internal to the storage ring. The kinematic range is $0.021 < x < 0.85$ and 0.8 GeV$^2 < Q^2 < 20$ GeV^2. The integral $\int_{0.021}^{0.85} g_1^{\mathrm{p}}(x)\,dx$ evaluated at Q_0^2 of 2.5 GeV^2 is $0.122 \pm 0.003(\text{stat.}) \pm 0.010(\text{syst.})$.

Deep-inelastic lepton-nucleon scattering is well established as a powerful tool for the investigation of nucleon structure. The measured structure functions have been successfully interpreted in terms of parton distributions. Scattering polarised leptons off polarised nucleons provides information on the spin composition of the nucleon. The major aim of the HERMES experiment is to determine the spin contributions of the various quark flavours to the spin of the nucleon from the combination of inclusive and semi-inclusive deep-inelastic polarised scattering data [1].

At centre-of-mass energies where weak contributions can be neglected, inclusive polarised deep-inelastic scattering is characterised by two spin structure functions: $g_1(x, Q^2)$ and $g_2(x, Q^2)$. Here Q^2 is the negative squared four-momentum of the exchanged virtual photon with energy ν and $x = Q^2/2M\nu$ is the Bjorken scaling variable, where M is the nucleon mass. The fractional energy transferred to the nucleon is given by $y = \nu/E$ for a lepton beam energy E. In leading order QCD the structure function g_1 is given by the charge weighted sum over the polarised quark (anti-quark) spin distributions Δq_f ($\Delta \bar{q}_f$):

$$g_1(x, Q^2) = \frac{1}{2} \sum_f e_f^2 \left(\Delta q_f(x, Q^2) + \Delta \bar{q}_f(x, Q^2) \right). \qquad (1)$$

Here e_f is the charge of the quark (anti-quark) of flavour f in units of the elementary charge and x is interpreted as the fraction of the nucleon light-cone momentum carried by the struck quark.

The focus of this letter is the proton structure function g_1^{p}, which provides a powerful constraint on the polarised quark distributions. The spin structure functions g_1 and g_2 can be determined from measurements of cross section asymmetries by combining data taken with a longitudinally polarised lepton beam and different spin orientations of the target nucleons. Scattering off a longitudinally polarised target or a transversely polarised target yields the asymmetries $A_{\parallel}$ and $A_{\perp}$, respectively. This letter reports on the results for g_1^{p} from the measurement of $A_{\parallel}$ using inclusive deep-inelastic scattering data collected in 1997. For this HERMES measurement the target was pure polarised hydrogen gas without dilution by other unpolarised atomic species, in contrast to previous measurements of g_1^{p} performed with solid targets at SLAC [2] and at CERN [3,4]. The target thickness, fraction of polarisable material, and the polarimetry are all significantly different for solid and gaseous targets.

The HERMES experiment is located in the East straight section of the HERA storage ring at the DESY laboratory in Hamburg. It uses the positron beam of 27.57 GeV energy with beam currents decreasing typically from 40 to 10 mA in eight hours. The positrons become transversely polarised by the emission of synchrotron radiation [5]. Longitudinal polarisation of the positron beam at the interaction point is achieved with spin rotators [6] situated upstream and downstream of the HERMES experiment. Equilibrium polarisation values in the range of 0.40 to 0.65 are reached with a rise-time of about 30 minutes. The beam polarisation is continuously measured using Compton back-scattering of circularly polarised laser light, achieving a statistical accuracy of typically 1% in 60 s. Two polarimeters are used, one measuring the transverse polarisation in the HERA West straight section [7] and the other measuring the longitudinal polarisation near the HERMES target [8]. After a normalisation by rise-time measurements they give consistent results for the entire running period [9]. The systematic uncertainties are respectively 3.4% and 4.3% of the measured values, dominated by the normalisation uncertainty of 3.3% as determined from the rise-time calibration. Data were accepted for this g_1^{p} analysis when the polarisation value was above 0.30; the average polarisation for this data was 0.55. For about 12% of the data, only the longitudinal polarimeter was operational.

The HERMES polarised proton target [10,11] is formed by injecting a nuclear-polarised beam of atomic hydrogen from an atomic beam source (ABS) [12] into a tubular open-ended storage cell. The cell confines the atoms in the region of the circulating beam and increases the probability of a positron-proton interaction by a factor of approximately one hundred compared with the free atomic beam. The storage cell is made of 75 μm thick aluminium, 400 mm long, and has an elliptical cross section 9.8 mm high and 29 mm wide. It is cooled to 100 K giving an areal density of 7×10^{13} atoms/cm^2. The proton polarisation in the atomic beam is above 0.95, while the

electron polarisation is less than 0.05. The beam also contains unpolarised hydrogen molecules at a level less than 1%. Due to depolarisation mechanisms which take place within the cell, the proton polarisation within the cell is slightly lower than in the atomic beam. These are spin exchange in atom-atom collisions, as well as depolarisation and recombination to molecules during interactions with the cell walls. The cell walls are coated with drifilm [13] to minimise the wall collision effects. There is good evidence that recombination is further suppressed by water adsorbed on the cell surface during normal operation [10,14]. A static magnetic field directed parallel to the positron beam axis is provided throughout the cell to define the quantisation axis. The operational field value is chosen to avoid resonant depolarisation of the protons by the pulsed magnetic field caused by the bunch structure of the HERA beam [15]. The spin direction in the target can be reversed in less than one second by selecting different spin states in the ABS. In operation the length of the time interval between reversals was randomised and was of the order of one minute. The atomic beam is injected into the storage cell via a side tube connected to its centre. The atoms diffuse to the open ends of the cell generating a triangular density distribution along the beam axis. The escaping gas is removed from the storage ring by high speed vacuum pumps. The residual gas in this vacuum system produces a further small source of unpolarised hydrogen molecules in the storage cell. The gas at the centre of the cell is sampled via a second side tube. Both the nuclear and electron polarisations of the atoms in this sample are measured with a Breit-Rabi polarimeter (BRP), and the atomic fraction with a target gas analyser (TGA) [11]. These measurements are made continuously achieving a statistical accuracy of typically 0.02 in 60 s.

The target proton polarisation P_T as seen by the positron beam is given by

$$P_T = \alpha_0 \left[\alpha_r + (1 - \alpha_r)\beta\right] P_T^{\mathrm{atom}}. \qquad (2)$$

Here P_T^{atom} is the proton polarisation in the atoms; its value was 0.92 ± 0.03. The atomic fraction α_0 accounts for the presence of the small number of molecules originating from the ABS and the residual gas in the vacuum system; it had a value of 0.99 ± 0.01. The fraction of atoms that are in the form of molecules produced by recombination is $(1 - \alpha_r)$. The value of α_r was 0.93 ± 0.04. The values of P_T^{atom} and α_r were corrected for the sampling efficiencies of the BRP and TGA. These corrections depend on the measured values and the knowledge of depolarisation mechanisms inside the cell. The quantity β is defined as the ratio of the polarisation of protons in molecules from recombination to the polarisation of protons in the atoms. Limits on this ratio $(0.2 \leq \beta \leq 1.0)$ were derived [14] from the relationship between the target polarisation and the corresponding asymmetry $A_{\|}$

measured when the recombination rate was high due to deliberately modified conditions at the cell surface. The resulting target polarisation P_T was 0.88 ± 0.04. The quoted values are averages over the data taking period and the uncertainties are systematic.

The HERMES detector is a forward spectrometer with a dipole magnet providing an integrated field of 1.3 Tm. The magnet is divided into two identical sections by a horizontal iron plate that shields the positron and proton beams from the magnetic field. Consequently, the spectrometer consists of two identical detector systems, and the minimum polar angle for the acceptance of scattered positrons is 40 mrad. The maximum angular acceptances are ±140 mrad vertically and ±170 mrad horizontally. For tracking in each spectrometer half, 42 drift chamber planes and 6 micro-strip gas chamber planes are used. Fast track reconstruction is achieved by a pattern-matching algorithm and a momentum lookup method [16]. For positrons with momenta between 3.5 and 27 GeV, the average angular resolution is 0.6-0.3 mrad and the average momentum resolution $\Delta p/p$ is 0.7-1.3% aside from bremsstrahlung tails. A detailed description of the spectrometer is found in Ref. [17].

The trigger is formed by a coincidence of signals from three hodoscope planes with those from a lead-glass calorimeter, requiring an energy of greater than 1.5 GeV to be deposited locally in the calorimeter. Positron identification is accomplished using the calorimeter, a scintillator hodoscope preceded by two radiation lengths of lead, a six-module transition radiation detector, and a $C_4F_{10}/N_2(70{:}30)$ gas threshold Čerenkov counter.

An adjustable two-stage collimator system is mounted upstream of the target cell to protect target and spectrometer from synchrotron radiation and from beam halo. The number of triggers originating from particles scattered from the storage cell walls was negligible. The luminosity is measured by detecting electron-positron pairs from Bhabha scattering off the target gas electrons, in two $NaBi(WO_4)_2$ electromagnetic calorimeters, which are mounted symmetrically on either side of the beam line.

The cross section asymmetry $A_{\|}$ was determined using the formula

$$A_{\|} = \frac{N^- L^+ - N^+ L^-}{N^- L_P^+ + N^+ L_P^-}. \qquad (3)$$

Here $N^+ (N^-)$ is the number of scattered positrons for target spin parallel (anti-parallel) to the beam spin orientation. The deadtime corrected luminosities for each target spin state are $L^{\pm}$ and $L_P^{\pm}$, the latter being weighted by the product of the beam and target polarisation values for each spin state. The luminosities were corrected for a small Bhabha cross section asymmetry caused by the typically 3% polarisation of the electrons in the target. The effect on $A_{\|}$ was determined to better than 0.2%.

The kinematic requirements imposed on the data were: $Q^2 > 0.8 \, \text{GeV}^2$, $0.1 < y < 0.85$, an energy of the hadronic final state $W > 1.8 \, \text{GeV}$, and a minimum calorimeter energy deposition of 3.5 GeV. After applying data quality criteria, 1.7×10^6 events were available for the asymmetry analysis. The data were analysed in bins of x and also y in order to include the effect of the variation of the virtual photon depolarisation factor D with y. For each bin and spin state the number of scattered positrons was corrected for e^+e^- background from charge symmetric processes. This correction was at most 8% in the bins with $x < 0.08$ and $y > 0.6$, and negligible for the remainder of the kinematic range. For the average positron identification efficiency of 99%, the average contamination of misidentified hadrons was negligible with values not greater than 1% in the lowest x bins. The asymmetry was further corrected for smearing effects due to the finite resolution of the spectrometer, which were determined by Monte Carlo simulations to be about 8% at low x and in the range of 2-3% at high x. QED radiative correction factors were calculated following the prescription given in Ref. [18]. The corrections were determined to be less than 8% at low x and high y, decreasing to less than 1% at higher x values. Both smearing and radiative corrections were calculated using an iterative procedure.

The structure function ratio g_1/F_1 is approximately equal to the longitudinal virtual photon asymmetry A_1. It was calculated in each (x, y) bin from the longitudinal asymmetry $A_{\parallel}$, corrected for the effects mentioned above, using the relation

$$\frac{g_1}{F_1} = \frac{1}{1+\gamma^2}\left[\frac{A_{\parallel}}{D} + (\gamma - \eta)A_2\right]. \qquad (4)$$

The virtual photon depolarisation factor $D = [1 - (1 - y)\epsilon]/(1+\epsilon R)$ depends on the ratio $R = \sigma_L/\sigma_T$ of longitudinal to transverse virtual photon absorption cross sections and is approximately equal to y. The kinematic factors are defined as $\epsilon = [4(1-y) - \gamma^2 y^2]/[2y^2 + 4(1-y) + \gamma^2 y^2]$, $\gamma = 2Mx/\sqrt{Q^2}$, and $\eta = \epsilon\gamma y/[1 - \epsilon(1 - y)]$. The magnitude of the transverse virtual photon absorption asymmetry A_2^{p} has been measured previously to be small [2]. Its contribution to $g_1^{\text{p}}/F_1^{\text{p}}$ is further suppressed by the factor $(\gamma - \eta)$ and was taken into account using a fit based on existing data [2,4]: $A_2^{\text{p}} = 0.5 \cdot x/\sqrt{Q^2}$.

The x dependence of the structure function ratio $g_1^{\text{p}}/F_1^{\text{p}}$ at the measured $\langle Q^2 \rangle$ for each value of x is shown in Fig. 1. The averaged values of x, Q^2, and the structure function ratio $g_1^{\text{p}}/F_1^{\text{p}}$ are listed in Table I. Fig. 2 shows a comparison of the measured $g_1^{\text{p}}/F_1^{\text{p}}$ values with recent results of previous experiments, E-143 [2] and SMC [4]. There is good agreement between these three sets of data, although the $\langle Q^2 \rangle$ values of E-143 and HERMES differ from those of SMC by a factor between five and ten. This demonstrates that there is no statistically significant Q^2 dependence of the ratio $g_1^{\text{p}}/F_1^{\text{p}}$ in the Q^2

range of these experiments. The spin structure function $g_1^{\text{p}}(x, Q^2)$ was extracted from the ratio $g_1^{\text{p}}/F_1^{\text{p}}$ using the relation $F_1 = F_2(1 + \gamma^2)/(2x(1 + R))$ with parameterisations of the unpolarised structure function $F_2^{\text{p}}(x, Q^2)$ [19] and $R(x, Q^2)$ [20]. The values of g_1^{p} at the measured x and Q^2 and after evolution to a common Q_0^2 of 2.5 GeV^2 are also given in Table I. The evolution was done under the assumption that the ratio of $g_1^{\text{p}}/F_1^{\text{p}}$ does not depend on Q^2. The same assumption was used to evolve the HERMES data to the Q_0^2 values as published by E-143 and SMC. As shown in Figs. 3a and 3b, the evolved HERMES data are in excellent agreement with both data sets. The apparent Q^2 dependence of g_1^{p} seen when comparing Fig. 3a with Fig. 3b entirely originates from the Q^2 dependence of the unpolarised structure functions F_2^{p} and R.
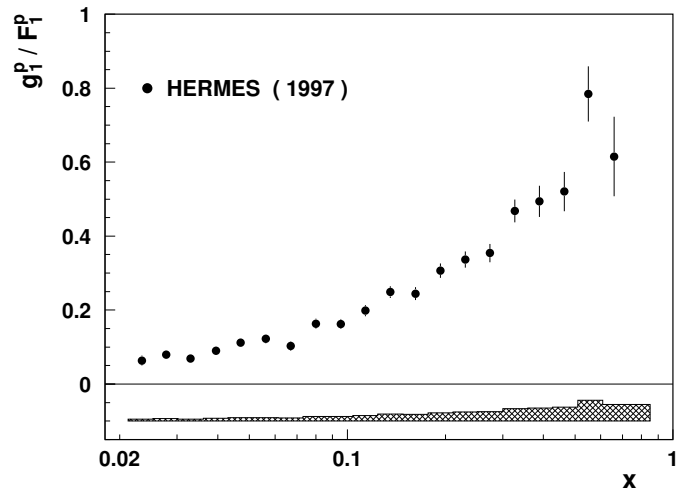

FIG. 1. The structure function ratio $g_1^{\text{p}}/F_1^{\text{p}}$ of the proton as a function of x, given for the measured $\langle Q^2 \rangle$ at each value of x. The error bars show the statistical uncertainties and the band represents the total systematic uncertainties.

The systematic uncertainty of this measurement of $g_1^{\text{p}}/F_1^{\text{p}}$, illustrated by the band in Fig. 1, is about 8% over the entire x range. The dominant sources of systematic uncertainties are the beam and target polarisation discussed above. An uncertainty of 2.5% is included to account for the uncertainty in the description of the spectrometer geometry. The uncertainty originating from the combined effects of smearing and QED radiative corrections is between 1% and 4%. The data were searched for possible systematic fluctuations in the measured asymmetry. This was carried out by dividing the data into sub-samples defined by various parameters, e.g. time, detector geometry and beam current. Within the statistical accuracy of the data no additional systematic effect was detected.
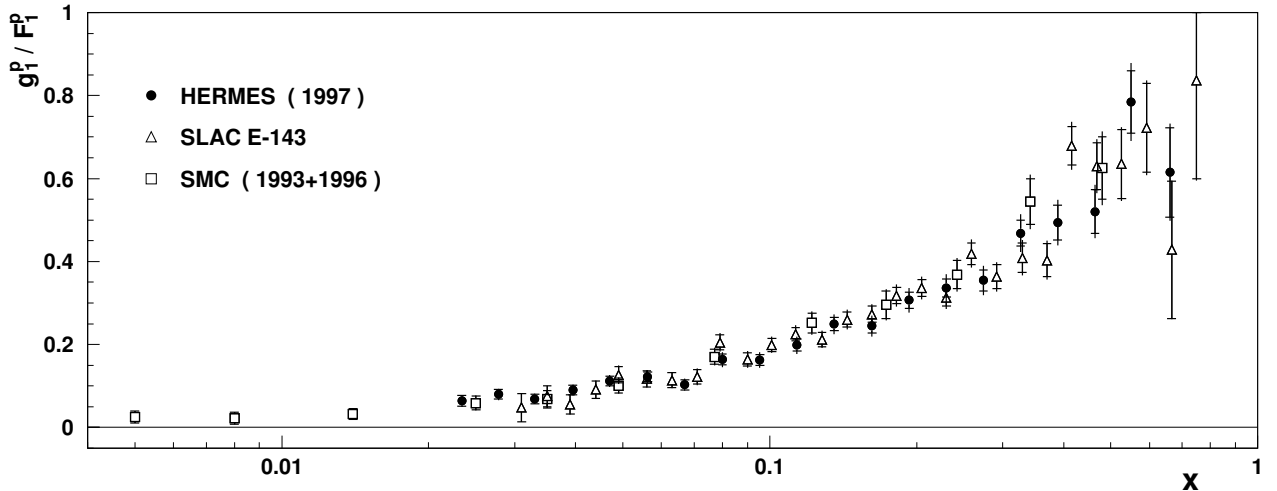
FIG. 2. Comparison of the data shown in Fig. 1 with recent results for g_1^p/F_1^p obtained at SLAC (E-143) and A_1^p at CERN (SMC) for $Q^2 > 1$ GeV^2. The inner error bars show the statistical uncertainties and the outer ones the quadratic sum of statistical and total systematic uncertainties.
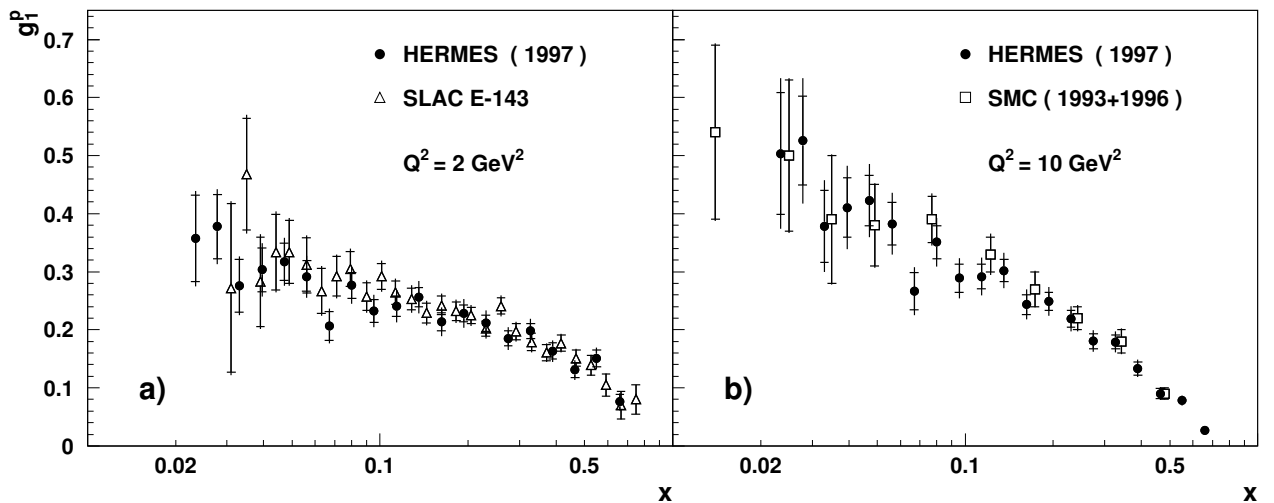

FIG. 3. The spin structure function g_1^p of the proton as a function of x. The HERMES data are evolved to a) $Q_0^2 = 2$ GeV^2 and b) $Q_0^2 = 10$ GeV^2 assuming g_1^p/F_1^p to be independent of Q^2. This measurement is compared to recent results for $Q^2 > 1$ GeV^2 from E-143 [2] and from SMC [4], the latter shown for $x > 0.01$ only. The error bars are defined as in Fig. 2.

The effect of the assumption for A_2^p on the extracted ratio g_1^p/F_1^p was estimated from an analysis of the variation within the statistical and systematic uncertainties of the recent A_2^p data of E-143 [2], the assumption $g_2 = 0$, and the use of the ansatz for g_2 given in Ref. [21]. The systematic uncertainty due to this effect was estimated to be at most 1.5%.

The values of the ratio g_1^p/F_1^p and also g_1^p derived from $A_{\parallel}$ depend on R. Using the uncertainties for R given in Ref. [20] changed the g_1^p/F_1^p (g_1^p) values by typically 3% (2%) and at most 5.5% (3.6%) at $x < 0.1$. In the HERMES kinematic region this uncertainty range of R covers the R measurement recently published for $x < 0.12$ [22]. Variations in the F_2^p parameterisation

calculated in Ref. [19] including the normalisation uncertainty of the F_2^{p} values of 0.7% resulted in changes in the extracted g_1^{p} of about 2.5%. The influence of R and F_2^{p} has not been included in the systematic uncertainty of the measurement and the values are given separately for each x bin in Table I.

TABLE I. Results on $g_1^{\mathrm{p}}(x,Q^2)/F_1^{\mathrm{p}}(x,Q^2)$, $g_1^{\mathrm{p}}(x,Q^2)$ and $g_1^{\mathrm{p}}(x,Q_0^2)$ evolved to $Q_0^2 = 2.5$ GeV^2 assuming $g_1^{\mathrm{p}}/F_1^{\mathrm{p}}$ to be independent of Q^2. The measured $\langle Q^2 \rangle$ values are given in GeV^2. For each x bin the uncertainties concerning R and F_2, $\delta(R)$ or $\delta(R, F_2)$, are listed separately. The systematic uncertainties are dominated by those of the beam and target polarisation which constitute a normalisation uncertainty only.

$\langle x \rangle$	$\langle Q^2 \rangle$	$g_1^{\mathrm{p}}/F_1^{\mathrm{p}}\pm$stat.$\pm$syst.$\pm\delta(R)$	$g_1^{\mathrm{p}}\pm$stat.$\pm$syst.$\pm\delta(R,F_2)$	$g_1^{\mathrm{p}}(x,Q_0^2)\pm$stat.$\pm$syst.$\pm\delta(R,F_2)$
0.023	0.92	$0.064 \pm 0.013 \pm 0.004 \pm 0.002$	$0.300 \pm 0.062 \pm 0.021 \pm 0.012$	$0.375 \pm 0.078 \pm 0.035 \pm 0.017$
0.028	1.01	$0.080 \pm 0.012 \pm 0.006 \pm 0.003$	$0.327 \pm 0.048 \pm 0.023 \pm 0.012$	$0.395 \pm 0.058 \pm 0.034 \pm 0.016$
0.033	1.11	$0.069 \pm 0.011 \pm 0.005 \pm 0.003$	$0.245 \pm 0.041 \pm 0.017 \pm 0.008$	$0.288 \pm 0.047 \pm 0.024 \pm 0.011$
0.040	1.24	$0.090 \pm 0.011 \pm 0.006 \pm 0.004$	$0.284 \pm 0.035 \pm 0.019 \pm 0.007$	$0.316 \pm 0.039 \pm 0.029 \pm 0.010$
0.047	1.39	$0.112 \pm 0.011 \pm 0.007 \pm 0.004$	$0.302 \pm 0.031 \pm 0.020 \pm 0.008$	$0.329 \pm 0.034 \pm 0.029 \pm 0.010$
0.056	1.56	$0.122 \pm 0.012 \pm 0.008 \pm 0.004$	$0.284 \pm 0.027 \pm 0.019 \pm 0.007$	$0.302 \pm 0.029 \pm 0.025 \pm 0.008$
0.067	1.73	$0.103 \pm 0.012 \pm 0.007 \pm 0.004$	$0.206 \pm 0.025 \pm 0.014 \pm 0.005$	$0.213 \pm 0.026 \pm 0.017 \pm 0.006$
0.080	1.90	$0.163 \pm 0.013 \pm 0.011 \pm 0.006$	$0.280 \pm 0.022 \pm 0.018 \pm 0.008$	$0.285 \pm 0.023 \pm 0.021 \pm 0.008$
0.095	2.09	$0.163 \pm 0.014 \pm 0.011 \pm 0.006$	$0.240 \pm 0.020 \pm 0.016 \pm 0.007$	$0.238 \pm 0.020 \pm 0.018 \pm 0.007$
0.114	2.26	$0.198 \pm 0.015 \pm 0.013 \pm 0.007$	$0.251 \pm 0.019 \pm 0.017 \pm 0.007$	$0.246 \pm 0.018 \pm 0.019 \pm 0.007$
0.136	2.44	$0.249 \pm 0.016 \pm 0.016 \pm 0.009$	$0.268 \pm 0.017 \pm 0.018 \pm 0.008$	$0.261 \pm 0.017 \pm 0.020 \pm 0.007$
0.162	2.63	$0.244 \pm 0.017 \pm 0.016 \pm 0.008$	$0.225 \pm 0.016 \pm 0.015 \pm 0.006$	$0.217 \pm 0.015 \pm 0.017 \pm 0.006$
0.193	2.81	$0.307 \pm 0.019 \pm 0.020 \pm 0.010$	$0.237 \pm 0.015 \pm 0.016 \pm 0.007$	$0.231 \pm 0.015 \pm 0.017 \pm 0.007$
0.230	3.02	$0.336 \pm 0.022 \pm 0.022 \pm 0.010$	$0.216 \pm 0.014 \pm 0.014 \pm 0.006$	$0.212 \pm 0.014 \pm 0.015 \pm 0.006$
0.274	3.35	$0.354 \pm 0.025 \pm 0.023 \pm 0.011$	$0.183 \pm 0.013 \pm 0.012 \pm 0.005$	$0.184 \pm 0.013 \pm 0.013 \pm 0.005$
0.327	3.76	$0.468 \pm 0.031 \pm 0.031 \pm 0.014$	$0.187 \pm 0.012 \pm 0.012 \pm 0.005$	$0.195 \pm 0.013 \pm 0.014 \pm 0.005$
0.389	4.25	$0.494 \pm 0.042 \pm 0.032 \pm 0.015$	$0.147 \pm 0.013 \pm 0.010 \pm 0.004$	$0.158 \pm 0.013 \pm 0.011 \pm 0.004$
0.464	4.80	$0.520 \pm 0.053 \pm 0.034 \pm 0.016$	$0.104 \pm 0.011 \pm 0.007 \pm 0.003$	$0.122 \pm 0.013 \pm 0.008 \pm 0.003$
0.550	5.51	$0.784 \pm 0.075 \pm 0.051 \pm 0.024$	$0.094 \pm 0.009 \pm 0.006 \pm 0.003$	$0.134 \pm 0.013 \pm 0.009 \pm 0.003$
0.660	7.36	$0.615 \pm 0.108 \pm 0.040 \pm 0.020$	$0.032 \pm 0.005 \pm 0.002 \pm 0.001$	$0.068 \pm 0.012 \pm 0.005 \pm 0.001$

Nucleon spin structure functions may be characterised in terms of sum rules which involve integrals of g_1 over x for a given Q_0^2 [23]. The integral of $g_1^{\mathrm{p}}(x)$ evaluated in the measured region $0.021 < x < 0.85$ and $Q^2 > 0.8$ GeV^2 is 0.122 ± 0.003(stat.)±0.010(syst.) at Q_0^2 of 2.5 GeV^2. In the integration the x dependence of F_1^{p} within the individual x bins was fully accounted for, whereas the x dependence of $g_1^{\mathrm{p}}/F_1^{\mathrm{p}}$ was treated in first order only. Possible Q^2 dependences not excluded by the present statistical accuracy were investigated using Q^2 dependent fits to the $g_1^{\mathrm{p}}/F_1^{\mathrm{p}}$ data according to Ref. [2] and a Q^2 dependence of A_1^{p} as parameterised by a next-to-leading order QCD analysis [24]. The effect on g_1^{p} was at most 8% at the lowest x and Q^2 values and was included in the systematic uncertainty of the integral. A contribution to the systematic uncertainty of 0.003 arose from the uncertainties due to R and F_2^{p} described above. The result obtained for the integral was compared with those from E-143 [2] and SMC [4], both calculated with the same integration scheme and for the kinematic range of HERMES. With respect to statistical uncertainties the agreement is better than 0.6σ and 1.2σ, respectively, well inside the normalisation uncertainty given by each experiment.

In summary, the proton structure function ratio $g_1^{\mathrm{p}}/F_1^{\mathrm{p}}$ was measured with good statistical and systematic precision. The results were obtained using an entirely different technique from that used in all previous experiments, involving a longitudinally polarised positron beam in a high energy storage ring and an internal polarised pure hydrogen gas target. The data are in good agreement with those obtained with solid targets at both similar and much higher Q^2 values, indicating that the systematic uncertainties are well understood for both techniques over the entire measured x range. Evolved to the same values of Q^2 all recent data on g_1^{p} and on its integral are consistent.

[1] HERMES Collaboration, K. Coulter *et al.*, DESY-PRC 90/01 (1990); DESY-PRC 93/06 (1993).

[2] E143 Collaboration, K. Abe *et al.*, Phys. Rev. Lett. **74** (1995) 346; Phys. Lett. **B364** (1995) 61; hep-ph/9802357 (1998) submitted to Phys. Rev. D.

[3] EMC Collaboration, J. Ashman *et al.*, Nucl. Phys. **B328** (1989) 1.

[4] SMC Collaboration, D. Adams *et al.*, Phys. Lett. **B329** (1994) 399; Phys. Rev. **D56** (1997) 5330; B. Adeva *et al.*, Phys. Lett. **B412** (1997) 414; CERN-EP/98-85 (1998) submitted to Phys. Rev. D.

[5] A.A. Sokolov and I.M Ternov, Sov. Phys. Doklady **8** (1964) 1203.

[6] D.P. Barber *et al.*, Phys. Lett. **B343** (1995) 436.

[7] D.P. Barber *et al.*, Nucl. Instrum. Meth. **A329** (1993) 79.

[8] A. Most, Proc. of the "12th International Symposium on High-Energy Spin Physics," edited by C.W. de Jager *et al.*, Amsterdam, The Netherlands, World Scientific (1997) 800.

[9] W. Lorenzon, Proc. of the Workshop "Polarised gas targets and polarised beams," edited by R. J. Holt and M.

A. Miller, Urbana-Champaign, USA, AIP Conf. Proc. 421 (1997) 181.

[10] J. Stewart, Proc. of the Workshop "Polarised gas targets and polarised beams," edited by R. J. Holt and M. A. Miller, Urbana-Champaign, USA, AIP Conf. Proc. 421 (1997) 69.

[11] B. Braun, Proc. of the Workshop "Polarised gas targets and polarised beams," edited by R. J. Holt and M. A. Miller, Urbana-Champaign, USA, AIP Conf. Proc. 421 (1997) 156.

[12] F. Stock *et al.*, Nucl. Instrum. Meth. **A343** (1994) 334.

[13] G.E. Thomas *et al.*, Nucl. Instrum. Meth. **A257** (1987) 32.

[14] H. Kolster, Ph.D. thesis, Universität München (1998).

[15] HERMES Collaboration, K. Ackerstaff *et al.*, DESY 98-058 (1998).

[16] W. Wander, Ph.D. thesis (in German), Universität Erlangen-Nürnberg (1996).

[17] HERMES Collaboration, K.Ackerstaff *et al.*, DESY 98-057 (1998), accepted by Nucl. Instrum. Meth. **A**.

[18] I.V. Akushevich and N.M. Shumeiko, J. Phys. **G20** (1994) 513.

[19] NMC Collaboration, M. Arneodo *et al.*, Phys. Lett. **B364** (1995) 107.

[20] L.W. Whitlow *et al.*, Phys. Lett. **B250** (1990) 193.

[21] S. Wandzura and F. Wilczek, Phys. Lett. **B72** (1977) 195.

[22] NMC Collaboration, M. Arneodo *et al.*, Nucl. Phys. **B483** (1997) 3.

[23] J.D. Bjorken, Phys. Rev. **148** (1966) 1467; ibid. **D1** (1970) 1376;
J. Ellis and R.L. Jaffe, Phys. Rev. **D9** (1974) 1444.

[24] M. Glück *et al.*, Phys. Rev. **D53** (1996) 4775.